# A SWEEP INTEGRATION SYSTEM USING FREQUENCY MODULATION

by

HAROLD MARTIN HEGGESTAD

Course VI May 21, 1962

(NESEP Program Thesis)

# A SWEEP INTEGRATION SYSTEM USING FREQUENCY MODULATION

by

HAROLD MARTIN HEGGESTAD

SUBMITTED IN PARTIAL FULFILLMENT OF THE
REQUIREMENTS FOR THE DEGREES OF
BACHELOR OF SCIENCE
AND
MASTER OF SCIENCE

at the

MASSACHUSETTS INSTITUTE OF TECHNOLOGY

May 21, 1962

Signature of Author _____
Department of Electrical Engineering

Certified by _____
Thesis Supervisor

Accepted by _____
Chairman, Departmental Committee on Graduate Students

# A SWEEP INTEGRATION SYSTEM USING FREQUENCY MODULATION

by

HAROLD MARTIN HEGGESTAD

Submitted to the Department of Electrical Engineering on May 21, 1962 in partial fulfillment of the requirements for the degrees of Bachelor of Science and Master of Science.

## ABSTRACT

A sweep integration system presently in use with weather radar is described; the stability limitations arising from the use of amplitude modulation in the system are explained. The design and construction of a basically similar sweep integrator is described, in which the use of frequency modulation removes the instability problem. The system contains a novel frequency modulator, consisting of a variable-phase-shift network in which the amount of phase shift is controlled by the modulating input signal.

It is demonstrated mathematically that if a series of these modulators are used to operate on a single carrier signal, the net frequency modulation of the carrier corresponds to the sum of the individually applied modulating signals.

Thesis Supervisor: William D. Jackson

Title: Assistant Professor of Electrical Engineering

# ACKNOWLEDGEMENT

The author wishes to acknowledge his gratitude for the patience and help of Mr. Kenneth Ultsch and Mr. Robert Splaine, who constructed the equipment; Mr. Sam Ricci, who drew the circuit diagrams; Miss Margot Fuller, who typed the report; and Professor William D. Jackson, the thesis supervisor, and Mr. Spiros Geotis, for their advice and assistance throughout the project.

# TABLE OF CONTENTS

## Figures

# CHAPTER I
# BACKGROUND

## I-A. Application of Sweep Integration to Weather Radar

The usefulness of weather radar in observing storms is limited by the statistical nature of the precipitation. Multiple reflections and refractions of radar waves by individual raindrops or snowflakes cause random fluctuations in the radar echoes, tending to obscure information about size, location and intensity of areas of precipitation.

Now, the true average value of a weather radar signal will change slowly, compared to radar pulse repetition rates. It would therefore seem reasonable that if a number of video return signals were added together and averaged, some of the fluctuating components would cancel out, while the true average value of the signal would remain nearly unchanged. Indeed, Kodaira[1] has examined and summarized the mathematical descriptions of the random fluctuations of weather signals, referring especially to the work of Marshall and Hitschfeld[2], who deduced that averaging $k$ independent weather signal intensity values will reduce the standard deviation of the measurements by $1/\sqrt{k}$ .

This adding and averaging process is called sweep integration, and it has been used successfully to suppress much of the statistical noise component of various types of periodic signals. One of the earliest contributions to the literature on the subject was written about eleven years ago by Harrington and Rogers[3], who described a basic sweep integration system, primarily for improving signal-to-noise ratio in digital read-out, in which a barrier-grid storage tube was used for the delay element.

There are several classified Philco Corporation reports[4] containing some information on sweep integration for military radars; some of it would be useful in a general way for application to weather radar. However, for purposes of this project, it would be desirable to avoid the use of any classified material.

The General Atronics Corporation[5] has published a brochure describing a phase-modulation type of sweep integrator. This has evidently been prepared for sales purposes, and it gives no detailed information about integrator design and construction.

## I-B. Kodaira's Sweep Integrator

Kodaira[6] has designed and built a Sweep Integrator for the Weather Radar Research Group at M.I.T. The following block diagram displays the essential features of the system:

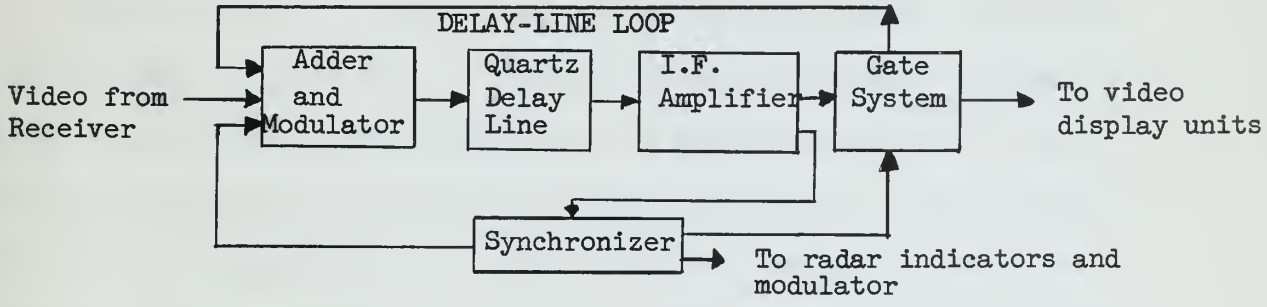


Figure I-1.
Block Diagram of Kodaira's Sweep Integrator

The quartz delay line, a product of Anderson Brothers, has a center frequency of 20 megacycles, main attenuation of 44 db, and delay of 2500 microseconds. The "Adder and Modulator" amplitude modulates a 20-mc carrier with the video from the radar receiver, which, after delaying, is amplified and detected by the I.F. strip. It is then gated back to the adder-modulator, where it is added to newly arrived video from the receiver, modulated, and delayed again. After the desired number of such circulations around the loop, the gate system passes the integrated video to the radar display units, and the integrating sequence begins again.

The Synchronizer produces the radar system trigger, and times the operation of the sweep integrator.

As the photographs and charts in Kodaira's report indicate, the sweep integrator brought about a profound improvement in the video signal-to-noise ratio; and it is, in fact, used every day with the SCR-615B weather radar unit.

It has, however, a rather severe stability limitation. The system is a closed loop; hence it will be stable only if the loop gain is maintained at unity, within certain fixed tolerances. As Kodaira points out(7), this permissible tolerance on the loop gain tightens progressively with increases in the number of loop circulations being performed. Therefore, even with automatic gain control of the I.F. amplifier, there is a limit to the number of sweeps which may be integrated before the system goes unstable. Kodaira's system is able to perform ten integrations with ease; considerably larger numbers of integrations can be accomplished, though only by means of extremely critical monitoring and adjustment of the amplifier and automatic gain control.

## CHAPTER II

## FM SWEEP INTEGRATION

### II-A. Motivation

The use of frequency modulation in a sweep integrator, as an alternative to the scheme described by Kodaira, has been reported in the literature[4,5]. Since the greatest problem with Kodaira's system is instability due to amplifier gain variation, it is natural to think of FM, where the problem could be neatly suppressed by simply limiting the signal at the desired amplitude level.

It appears, however, that very little work has been done in the particular application of FM sweep integration to weather radar. Such a system would be very desirable, in that increasingly greater numbers of circulations around the delay loop in the integrator could be tried; and this would, at least in theory, give progressively better signal-to-noise ratios. Obviously, this would greatly enhance the usefulness of weather radar observations.

The design and development of an FM integrator system to operate with the AN/CPS-9 weather radar unit is the topic of this thesis report.

### II-B. A Phase-Shift Angular Modulator

One limiting feature of Kodaira's sweep integrator is the necessity to detect and re-modulate the video each time it circulates around the loop. It seems probable that a certain amount of noise and distortion is thus introduced during each circulation; accordingly a method of avoiding this source of error would be desirable.

The standard method of producing an angle-modulated signal is to vary the reactance of an oscillator tank circuit; but this method requires the

undesirable repeated detection and remodulation mentioned above. However, consider passing a carrier signal through a modulator consisting of a variable-phase-shift network, as in the diagram below, where the applied modulating signal $v_m(t)$ controls the amount of phase shift:

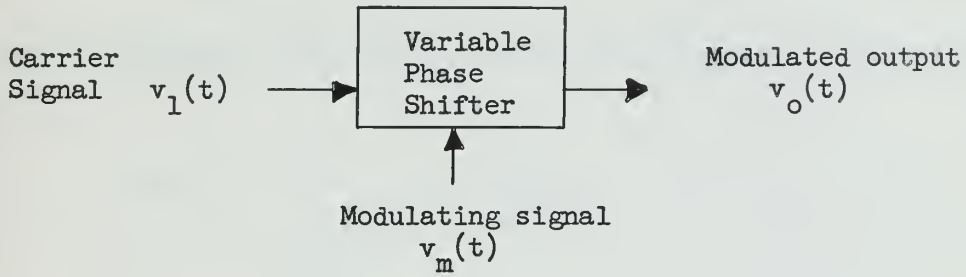


Figure II-1
Variable-Phase-Shift System

If this is possible, and if the process is linear, then a device has been realized with which several signals could be <u>added</u> by using each signal successively to modify the modulation of the carrier, $v_1(t)$. After these successive operations, in other words, the modulation of the carrier would correspond to the <u>sum</u> of the signals that were individually applied to the modulator.

It will be demonstrated that this unusual device is indeed realizable <u>and linear</u>, provided that certain restrictions are observed.

## II-B. A Phase-Shift Angular Modulator

### II-B-1. Mathematical Expressions for Angle-Modulated (i.e., Frequency- or Phase-Modulated) Signals

Given a modulating signal

$$e_m = E_m \cos\omega_m t$$

which is to frequency-modulated a carrier at frequency $\omega_c$, we have after modulation

$$\omega(t) = \omega_c + k_f E_m \cos\omega_m t$$

$$= \frac{d\phi(t)}{dt} \quad ,$$

where $\omega(t)$ is the instantaneous frequency, $\phi(t)$ is the instantaneous phase, and $k_f$ is a constant of the modulator.

Clearly,

$$\phi(t) = \int_0^t \omega(t)\, dt$$

$$= \omega_c t + k_f \frac{E_m}{\omega_m} \sin \omega_m t \quad .$$

The FM signal may thus be expressed as

$$e_{fm} = E_c \sin\left(\omega_c t + k_f \frac{E_m}{\omega_m} \sin\omega_m t\right) \quad ;$$

if we define a deviation ratio

$$\lambda_f = k_f \frac{E_m}{\omega_m} \quad ,$$

we may express the FM signal in the more general form

$$e_{fm} = E_c \sin(\omega_c t + \lambda_f \sin\omega_m t) \quad . \qquad \text{(II-1)}$$

If now we apply the same modulating input to a phase modulator, we will have

$$\phi(t) = \omega_c t + k_p E_m \cos\omega_m t \quad ,$$

where $\phi(t)$ is again the instantaneous phase, and $k_p$ is a constant of the phase modulator. The PM signal may be expressed in the general form

$$e_{pm} = E_c \sin(\omega_c t + \lambda_p \cos\omega_m t) \quad , \qquad \text{(II-2)}$$

where we have defined

$$\lambda_p = k_p E_m \quad .$$

Notice that FM and PM signals may be expressed in precisely the same form (Eqns. II-1 and II-2); and, in fact, a phase modulator may be used to produce frequency modulation, if the modulating signal is first integrated to introduce the factor $1/\omega_m$ .

This relationship is examined in another aspect, in Appendix A.

## II-B-2. A Variable-Phase-Shift Network as a Phase Modulator

Suppose that we have a capacitor with a time-varying capacitance $C(t)$ , and that we use it in a simple R-C phase shift network:

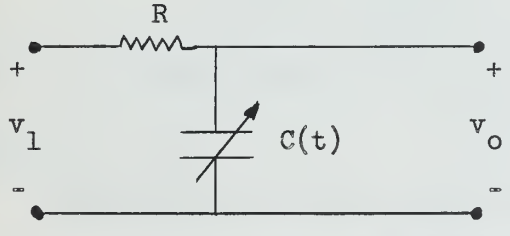


Figure II-2
Variable-Phase-Shift Network

Let the input be $v_1 = V_1 \sin\omega_1 t$ ; and let us find under what conditions we would obtain a phase-modulated output $v_o(t) \cong k_1 V_1 \sin\left[\omega_1 t + k_2\, C(t)\right]$ . This question may be answered as follows: A complete solution of the network shows that the output consists of a steady-state component and a starting transient. The steady-state component is found in a straightforward manner to be

$$v_o(t) = \frac{V_1}{\sqrt{1 + \omega_1^2 R^2 C^2(t)}} \sin\left[\omega_1 t - \tan^{-1} \omega_1 RC(t)\right] \qquad \text{(II-3)}$$

By expanding $\tan^{-1}\chi$ , it is easily shown that $\tan^{-1}\chi \cong \chi$ within 1% for $\chi \leq 0.17$ ; hence we have the desired result ,

$$v_o(t) \cong k_1 V_1 \sin\left[\omega_1 t - \omega_1 RC(t)\right] \quad ,$$

$$\text{within } 1\% \text{ for } \omega_1 RC(t) \leq 0.17 \; . \qquad \text{(II-4)}$$

Suppose now that the capacitor $C(t)$ is a Semicap (6.8SC20, International Rectifier Corporation). This is a semiconductor diode; when back-biased, it has a depletion-layer capacitance given in micro-microfarads by

$$C(t) = k_c (V)^{-1/2} \quad ,$$

where $k_c$ is approximately 16, and $V$ is the applied d.c. (or slowly-varying) back bias.

Expanding $C(t)$ in a Taylor series about the operating point $V = e_o$ , and defining the small-signal voltage $v_b = V - e_o$ , we have

$$C(t) = k_c e_o^{-1/2} - \frac{1}{2} k_c e_o^{-3/2} v_b + \frac{3}{8} k_c e_o^{-5/2} v_b^2 - \cdots\cdots$$

$$\cong k_c e_o^{-1/2} - \frac{1}{2} k_c e_o^{-3/2} v_b \quad . \qquad \text{(II-5)}$$

We wish to know the range of $v_b$ for which the linear approximation, Eqn. II-5 above, is valid within 1% . This may be found with good accuracy by comparing Eqn. II-5 with the quadratic approximation above; accordingly, we write

$$1\% = \frac{C_{quadratic} - C_{linear}}{C_{quadratic}} \quad , \quad \text{or}$$

$$\frac{1}{100} = \frac{\frac{3}{8} k_c e_o^{-5/2} v_b^2}{k_c e_o^{-1/2} - \frac{1}{2} k_c e_o^{-3/2} v_b + \frac{3}{8} k_c e_o^{-5/2} v_b^2} \quad .$$

Solving this equation for $v_b$ , we see that, for a Semicap ,

$$C(t) \cong 16\, e_o^{-1/2} - 8\, e_o^{-3/2} v_b \qquad \text{(II-6)}$$

within 1% , for $v_b \leq 0.15\, e_o$ .

This restriction, and the earlier one that $\omega_1 RC(t) \leq 0.17$, determine the permissible region of operation of the network.

The biasing and input circuitry that must be used with the phase shifting network will be discussed in detail in a later section.

## II-C. n - Fold Angular Modulation of a Carrier

Postulate an ideal angular modulator, which takes a carrier input

$$e_c = E_c \sin\omega_c t$$

and a modulating input

$$e_m = E_m \sin\omega_m t$$

and produces an output of the form

$$e = E_c \sin(\omega_c t + \lambda \sin\omega_m t) \quad . \tag{II-7}$$

In Appendix B it is demonstrated, subject to certain restrictions and approximations, that this modulator may be used to perform n-fold angular modulation linearly, as shown in the following diagram:

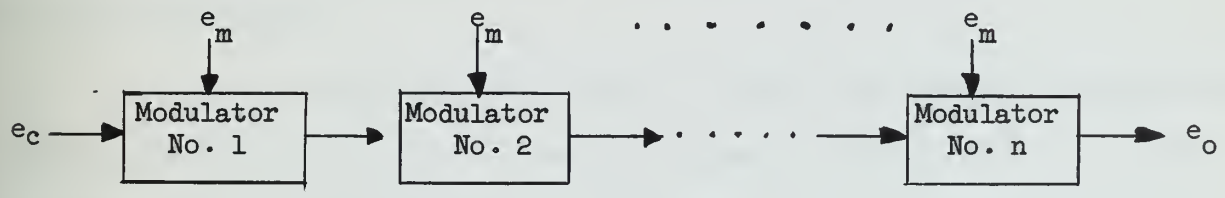


Figure II-3.
n-Fold Angular Modulation

It is shown, in other words, that the final output $e_o$ is equivalent to the output obtained by modulating once with a modulating signal n times as great in amplitude.

The procedure used in Appendix B is to expand the expression II-7 above in terms of Bessel functions, then to treat each component in the expansion as a separate carrier in the second modulation. This expansion and re-modulation is extended by iteration to n-fold modulation.

It is found that this process is permissible provided that almost all the power in the final output signal is contained in the carrier-frequency component and the first pair of sidebands. This is done by restricting the value of the parameter $\lambda$ in the angular-modulated signal (Eqn. II-7), so that

$$\lambda \leq 0.28 \qquad \text{(II-8)}$$

for a single modulation, and

$$\lambda \leq 0.28/n \qquad \text{(II-9)}$$

for n-fold modulation.

It may be noted that (II-8) above is almost the same as the restrictions Armstrong derived to insure less than 10% harmonic distortion in his indirect FM generator.[12] Furthermore, the restriction (II-8) is closely related to the condition for frequency modulation with a sum of a number of frequency components as a modulating input.[11]

## II-D. A Frequency-Modulation Sweep Integrator

The sweep integrator which is the subject of this thesis report, to be used with the AN/CPS 9 weather radar, has the form shown in the following simplified block diagram:

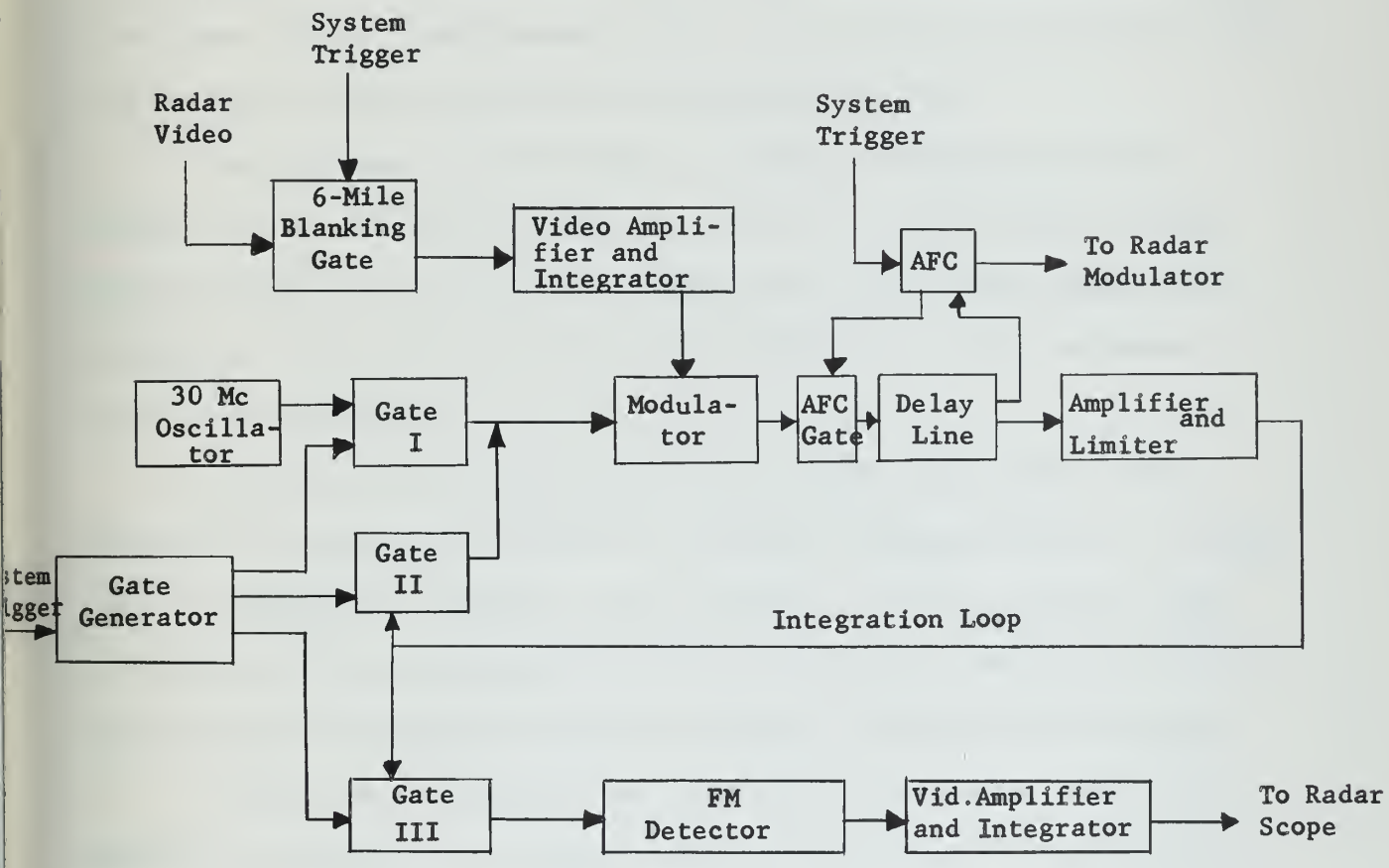


Figure II-4
FM Sweep Integrator

At the start of an integration cycle, the carrier is passed through Gate I for the duration of one period of the radar pulse repetition frequency. In the modulator it is frequency-modulated by the radar video signal; it is

delayed, amplified, and limited. Gate II passes the delayed FM signal back to the modulator, and the modulation and delaying process is repeated the desired number of times. Gate II is then closed; Gate III is opened during one PRF period to pass the signal through the FM detector and video amplifier to the radar scope. Simultaneously Gate I passes the 30 Mc oscillator output into the loop to begin the second sweep integration cycle.

The gate generator determines the number of sweeps to be added together in each integration cycle; if n sweeps are to be added, the gate generator selects every $n^{th}$ system trigger pulse, and produces appropriate waveforms to operate the three gates. The range of n in this equipment is from one to seventy-five.

The modulator in the system is the variable-phase-shift network described in Section II-B. Since it is actually a phase modulator, the radar video is integrated in the input video amplifier, in order that the signal in the loop will be frequency-modulated. The six-mile blanking gate blocks the large-amplitude transmitted pulse and ground clutter from the system.

The automatic frequency control circuit corrects the radar pulse repetition frequency to correspond exactly to the length of the delay line.

## CHAPTER III

## CIRCUITS AND EQUIPMENT IN THE FM SWEEP INTEGRATOR

### III-A. The 30 Megacycle Oscillator

The oscillator, a compact printed-circuited unit (Model FO-1B) made by International Crystal Manufacturing Co., uses a 0.01% -accuracy crystal. It has an output impedance of 18 kilohms, and a 5:1 step-down transformer is used at the oscillator output to feed into about 100 ohms impedance.

### III-B. The Gating System (Figures III-4 and III-5 , pages 40 and 41 )

#### III-B-1. The Six-diode Gates

The gates are patterned after a description in Millman and Taub,[13] and are similar to those used by Kodaira.

Essentially, they have the following form:

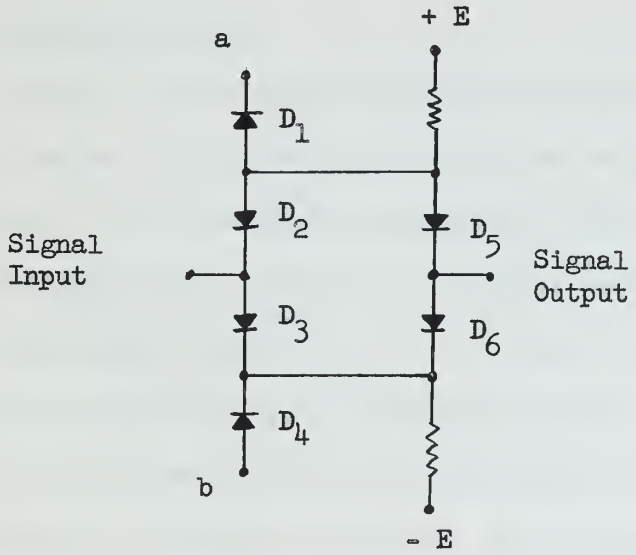


Figure III-1
Six-diode gate

(The additional resistors in the actual circuits, Figure III-5 , page 41 , are for biasing purposes; the potentiometer permits d.c. balance adjustment.)

In the case of Gates I and III, the biasing is such that diodes $D_3$, $D_4$, $D_5$, and $D_6$ are normally cut off; if a positive pulse is applied at input a and a negative pulse is applied at b, then the four diodes conduct, and a conducting path is provided from the signal input to the signal output.

Gate II is just the reverse; it is biased in such a way that $D_3$, $D_4$, $D_5$, and $D_6$ are normally conducting. The application of a negative pulse at a and a positive pulse at b cuts off the four diodes, and the path from the signal input to the signal output is broken.

III-B-2. The Gate Generator

The radar system trigger pulse train, which has a frequency of 931.2 per second (corresponding to 100 miles of radar range), is fed to a series of three ordinary frequency-dividing blocking oscillators (Figure III-4 , page 40 ). Their count-down ratios are variable, with maximum values of 5:1, 5:1, and 3:1 respectively. Thus the overall count-down ratio may be varied between 1:1 and 75:1.

The pulses selected by the count-down system are used to trigger a monostable blocking oscillator, whose unstable state is adjusted to 1074 microseconds in duration (equal to 100 miles of radar range, the period of the system trigger pulse train). The plate outputs

of this multivibrator are the waveforms required for the operation of the gates. Since the three gates would load the multivibrator plate outputs excessively, two cathode followers were provided for each of the gates at the control-pulse inputs.

III-C. Video Input Circuitry (Figure III-6 , page 42 )

The transmitted pulse and the ground clutter are of much larger amplitude than the rest of the video, and would have adverse effects on the sweep integrator. Most of this disturbance occurs in the first six miles, or about 70 microseconds, of the video.

In the circuitry shown in Figure III-6, page 42 , the system trigger is fed to a monostable multivibrator, which stays in its unstable state for about 70 microseconds; its plate outputs are applied through cathode followers to a diode gate similar to those already described, which blocks the first 70 microseconds of the video.

The video must, as mentioned earlier, be integrated at some time during the cycle. But the bandwidth of the video extends from approximately one kilocycle to one megacycle; integration of this entire spectrum would attenuate the higher-frequency components so much that they would be lost in the noise. Therefore, the integrator in the video input amplifier integrates only the portion of the video between 1 Kc and 30 Kc; the rest of the integration is done at the system output.

## III-D. The Variable-Phase-Shift Modulator and AFC Gate

The R-C variable-phase-shift network described in Chapter II is used in this equipment, operated in such a way that it produces phase modulation. The details of the circuit are shown in Figure III-7, page 43 .

The Semicap is back-biased by about ten volts; the 1-henry inductor isolates the circuit from the biasing voltage divider.

The video signal is applied as a varying bias to the Semicap through the 50 microhenry inductor, an intermediate size which passes the video but presents 10,000 ohms impedance to the 30-megacycle carrier. The RC differentiator immediately after the Semicap passes the 30-megacycle signal, but blocks most of the video.

The AFC gate passes the 30-mc signal through diode $D_2$, which is normally forward-biased; as will be described in a succeeding section, the AFC circuit applies a positive pulse at intervals through diode $D_1$, which cuts off diode $D_2$ and blocks the 30-mc signal for the duration of the pulse.

## III-E. The Delay Line, Amplifier-Limiter, and FM Detector

These three items were purchased commercially. The delay line was made by Anderson Brothers, Inc. (Model 798); it is an ultrasonic quartz delay line, which operates at a fixed center frequency of 30 megacycles. Its main attenuation is 46 db, and its spurious response is -44 db. The delay is 1074 microseconds, which is equal to the period of the AN/CPS 9 radar pulse repetition.

The amplifier-limiter, made by Applied Research, Inc. (Model UH-6(C)-30), has a center frequency of 30 megacycles, gain of 50 db, and a bandwidth of 10 megacycles.

The FM discriminator, also made by Applied Research, Inc. (Model UH-1(C)-30/5D), has a bandwidth of 6 megacycles.

## III-F. The AFC System (Figure III-8, page 44)

The period of the radar pulse repetition must correspond precisely to the time delay through the quartz delay line. If this were not so, then the video signals applied to the modulator during successive sweeps would be displaced with respect to each other. The function of the automatic frequency control system is to compare the delay time with the pulse repetition period, and to insure that they are exactly equal.

In the AN/CPS-9 weather radar unit the system trigger is produced by frequency-dividing and shaping the output of a 93.120 kilocycles/second crystal oscillator, to yield a train of positive pulses at the pulse repetition frequency of 931.2 per second. The AFC system replaces the crystal oscillator with a master timing oscillator, whose frequency may be varied slightly by the d.c. output of a coincidence circuit, which is very similar to that used by Kodaira[14] (see Figure III-8, page 44).

Tubes V1, V2, and V3 are blocking oscillators, which take the system trigger as an input and generate two additional pulses, as shown schematically in Figure III-2.

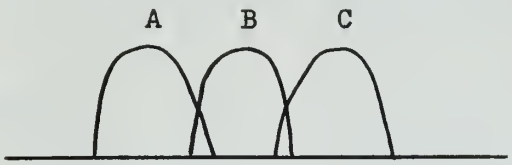


Figure III-2
Time Relationship of AFC Pulses

Pulse B (from blocking oscillator V2) is applied to diode D1 in the AFC Gate (Figure III-7, page 43 ), to cut off for about one and a half microseconds the 30-megacycle signal input to the quartz delay line. After the delay line, this pulse is recovered by the detector in the I.F. amplifier, amplified by pulse amplifiers V8 and V9, and applied as a trigger pulse to blocking oscillator V7, to produce a negative pulse output B' . Tube V4 keeps pulse B' locked between pulses A and C , as follows: if B' moves toward A or C , the two halves of tube V4 conduct unequally, causing a change in the d.c. bias applied to the reactance tube V5 in the master timing oscillator. The oscillator frequency is thus changed enough to move pulse B' back between A and C , constraining the pulse repetition period to be equal to the delay time.

The AFC characteristics are shown graphically in Figure III-9, page 45.

# CHAPTER IV

## OPERATION OF THE FM SWEEP INTEGRATOR

### IV-A. The Gating System

Figures IV-1 and IV-2, page 21 , show the operation of the six-diode gates in the system. The upper trace in both photographs shows the radar system trigger signal, for time comparison, showing that the gates correspond to the integration of fifteen sweeps. A three-kilocycle signal is applied to the gates, for easy visibility of the signal on the photographs.

Figure IV-3, page 21 , shows the behavior of the thirty-megacycle carrier signal as it is circulated around the loop. In the first interval the carrier is injected into the loop from the oscillator; thereafter, as it circulates around the loop, its amplitude is increased progressively until near the end of the cycle limiting begins to occur.

### IV-B. The Variable-Phase-Shift Modulator

Figure IV-4, page 21 , shows the result of a single modulation of the carrier by the variable-phase-shift network, using the partial integrators in both the input and output video amplifiers. The upper trace shows the input signal, and the lower trace shows the detected output. The 60-cycle disturbance visible in the output signal is due to a fault in the output video amplifier.

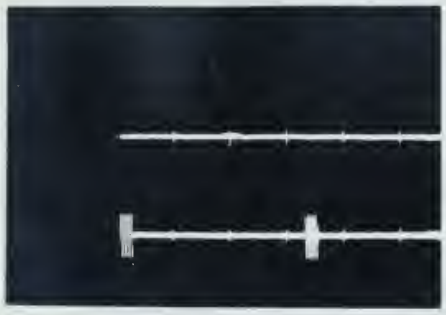

Fig. IV-1 Gates I and III

5 millisec/cm
Upper trace: 50 v/cm
Lower trace: 1 v/cm

Fig. IV-2 Gate II

5 millisec/cm
Upper trace: 50 v/cm
Lower trace: 1 v/cm

Fig. IV-3 Carrier Behavior

2 millisec/cm
1 v/cm

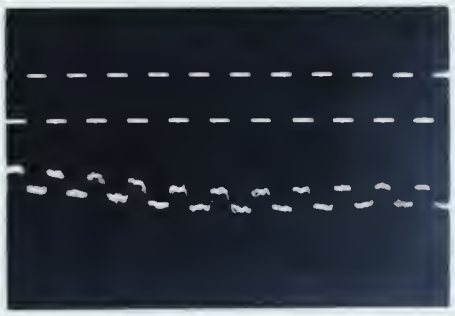

Fig. IV-4 Single Modulation

1.4 millisec/cm
Upper trace: 0.5 v/cm
Lower trace: 1 v/cm

As shown in Section II-B-2, the variable-phase-shift network operates as a linear phase modulator only for low-level modulation; that is, the modulating input voltage level must be less than 15% of the fixed bias applied to the Semicap, or about 1.5 volts. The resulting frequency deviation is so small, however, for a single modulation of the carrier, that it would scarcely be detected by the discriminator. The 0.8-volt square wave input in Figure IV-4, after amplification by the input video amplifier, drives the Semicap far out of the region of linear phase modulation. That is the primary cause of the noise and distortion of the modulated and detected output signal in Figure IV-4.

The discriminator in the system is badly mistuned, and must be returned to the factory for proper adjustment. Its characteristic is quite nonlinear, and therefore it further distorts the detected output in Figure IV-4.

## IV-C. The AFC System

The operation of the AFC gate described in Section III-F produces the lower signal in Figure IV-5, page 23, when the integration loop is open. This signal is detected, and is amplified by the two pentode amplifiers in the AFC system to produce the coincidence-circuit trigger shown in the upper trace of Figure IV-5.

Figure IV-6, page 23, illustrates the operation of the coincidence circuit when the radar system trigger signal is "locked-on", with its period exactly equal to the time delay of the quartz delay line. The upper trace of Figure IV-6 is the plate waveform of the upper triode in the coincidence

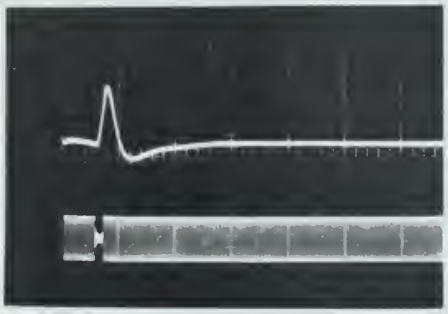

Fig. IV-5 AFC Trigger Pulses

10 microsec/cm
Upper trace: 50 v/cm
Lower trace: 1 v/cm

Fig. IV-6 "Locked-on" AFC

1 microsec/cm
Upper trace: 200 v/cm
Middle trace: 50 v/cm
Lower trace: 200 v/cm

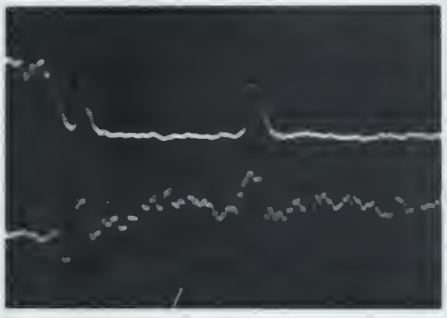

Fig. IV-7 Sweep Integration

20 microsec/cm
Upper trace: 10 v/cm
Lower trace: 2 v/cm

Fig. IV-8 Sweep Integration with Frequency Mismatched

20 microsec/cm
Upper trace: 10 v/cm
Lower trace: 2 v/cm

circuit (referring to the circuit diagram, Figure III-8, page 44 ), the lower trace of Figure IV-6 is the plate waveform of the lower triode of the coincidence circuit, and the center trace of Figure IV-6 is the grid waveform of both triodes. If any drift occurs in the master oscillator, the coincidence circuit automatically corrects the oscillator to keep the center signal between the other two.

The characteristics of the AFC circuit are shown in Figure III-9, page 45.

## IV-D. Sweep Integration

Figure IV-7, page 23, shows the result of actual operation of the sweep integrator. The upper trace is the short-range "ground clutter" video signal from the CPS-9 radar; the lower trace is the result of the integration of fifteen sweeps. It is noisy and distorted, for reasons to be described below; and it has 60-cycle disturbance, due again to faulty operation of the output video amplifier.

The signals of Figure IV-7 were obtained without the use of the AFC system; the radar trigger frequency was adjusted manually to the correct value. Figure IV-8, page 23, shows the effect of a slight misadjustment of the trigger frequency: the modulation occurred at a different time during each successive sweep, resulting in the series of adjacent pulses on the lower trace.

The malfunctioning of the AFC system was the reason that the results described in Sections IV-B and IV-C were obtained with the integration loop open. This malfunctioning was caused by the gates, which must be redesigned.

It is clear from Figures IV-1 and IV-2 that the gates inject undesirable pulses into the system when they turn on and off; this is shown more plainly by Figure IV-9, page 26, the output of Gate II when no signal input is applied. It was felt that the bandpass and limiting characteristics of the I.F. amplifier would remove these disturbances from the loop; that this is not so is shown clearly in Figure IV-10, page 26, the output of the I.F. strip. A portion of this signal is shown on an expanded time scale in Figure IV-11, page 26. The short AFC pulse of negative amplitude modulation seen in Figure IV-5 ought to appear in Figure IV-11, but it is swamped by the pulse disturbances, and hence cannot be used to trigger the coincidence circuit for automatic frequency control.

Since the signals applied to the gates are no more than one or two volts in magnitude, it ought to require pulses of no more than five or six volts to shut them off. But the gates in this system require driving pulses of thirty to thirty-five volts to operate properly, as shown in Figure IV-12, page 26; it is clear that the biasing arrangements of the gates are faulty.

Fig. IV-9 Gate II Output

1 millisec/cm
5 v/cm

F. F. [illegible]

2 millisec/cm
2 v/cm

Fig. IV-11 Expanded I.F. Output

20 microsec/cm
2 v/cm

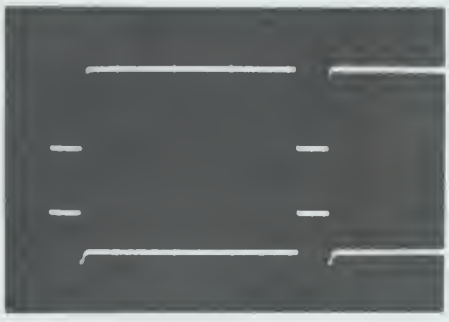

Fig. IV-12 Gate II Driving Waveforms

2 millisec/cm
Upper trace: 20 v/cm
Lower trace: 50 v/cm

# CHAPTER V
## CONCLUSIONS

Narrow-band FM, in which there are a carrier component and only one pair of sidebands, is linear with respect to additional frequency modulation. A carrier signal may be frequency-modulated repeatedly with an arbitrary number of modulating input signals, so long as the deviation ratio is appropriately restricted, and the net modulation of the resulting narrow-band FM signal will correspond to the sum of all the modulating input signals. A formal demonstration of this conclusion is given in Appendix B.

The results described in Section IV-D indicate that n-fold angular modulation is indeed possible. Conclusive proof of the linearity of the process depends, however, upon satisfactory operation of the rest of the sweep integration system.

Chapter IV indicates the directions in which further work on the equipment shall proceed. Obviously the output video amplifier must be improved, and the variable-phase-shift circuit may have to be modified slightly. Work is progressing on the redesigning of the gates, the major fault in the system; smaller and faster diodes will be used, the biasing arrangements will be modified, and the driving waveforms will be greatly reduced in amplitude.

After this is accomplished, the AFC system will operate properly; the repeated angular modulation will then be investigated quantitatively, and the FM sweep integrator will be compared in detail with the present AM system.

An account of the final results of this project will be included in a future Quarterly Technical Report of Weather Radar Research, to be published at M.I.T. under Signal Corps Contract No. DA 36-039-SC75030.

## APPENDIX A

## Phase and Frequency Modulation

A general angle-modulated wave is expressed as

$$e = E_c \sin(\omega_c t + \lambda \sin\omega_m t) \ . \qquad \text{(A-1)}$$

The instantaneous phase is clearly

$$\phi(t) = \omega_c t + \lambda \sin\omega_m t \ ,$$

and the instantaneous frequency is

$$\omega(t) = \frac{d\phi(t)}{dt} = \omega_c + \lambda \omega_m \cos\omega_m t \ .$$

We define the instantaneous <u>frequency deviation</u> $\omega_d$ :

$$\omega_d = \omega(t) - \omega_c$$

$$= \lambda \omega_m \cos\omega_m t \ . \qquad \text{(A-2)}$$

Now, a <u>detector</u> for an angle-modulated signal, such as a discriminator or a ratio detector, (ideally) produces an output with the equation

$$e_o = k_d \omega_d = k_d \lambda \omega_m \cos\omega_m t \ , \qquad \text{(A-3)}$$

where $k_d$ is a constant of the detector.

This is the key equation; notice the appearance of the factor $\underline{\omega_m}$ . If the angle-modulated signal (Eqn. A-1) had been an FM signal, with $\lambda = \lambda_f = k_f \frac{E_m}{\omega_m}$ , then the factor $\underline{\omega_m}$ would be cancelled; the detector output (Eqn. A-3) would be proportional to the original modulating input.

But if the angle-modulated signal (Eqn. A-1) had been a PM signal, with deviation ratio $\lambda = \lambda_p = k_p E_m$, then the factor $\omega_m$ would not be cancelled; clearly, the detector output would be proportional to the derivative of the modulating input signal.

## APPENDIX B

## n-Fold Angular Modulation of a Carrier

The output of the ideal angular modulator described in Chapter II was expressed as

$$e = E_c \sin(\omega_c t + \lambda \sin\omega_m t) .$$

It is easily shown that this expression may be expanded in the following form:

$$\begin{aligned} e = {} & J_o(\lambda)\, E_c \sin \omega_c t \\ & + J_1(\lambda)\, E_c \left[\sin(\omega_c + \omega_m)t - \sin(\omega_c - \omega_m)t\right] \\ & + J_2(\lambda)\, E_c \left[\sin(\omega_c + 2\omega_m)t - \sin(\omega_c - 2\omega_m)t\right] \\ & + J_3(\lambda)\, E_c \left[\sin(\omega_c + 3\omega_m)t - \sin(\omega_c - 3\omega_m)t\right] \\ & + \cdots\cdots\cdots , \end{aligned} \tag{B-1}$$

where $J_n(\lambda)$ is the Bessel function of the first kind and $n^{th}$ order, with argument $\lambda$. Any calculations beyond this point are mathematically intractable, because of the transcendental nature of the Bessel functions. Therefore suitable approximations to the Bessel functions will now be derived.

A general formula for the Bessel function of the first kind and $n^{th}$ order is as follows:

$$J_n(\lambda) = \frac{\lambda^n}{2^n n!} \left[ 1 - \frac{\lambda^2}{2(n+2)} + \frac{\lambda^4}{2(4)(2n+2)(2n+4)} - \frac{\lambda^6}{(2)(4)(6)(2n+2)(2n+4)(2n+6)} + \cdots \right] . \tag{B-2}$$

It is clear that the higher-order terms rapidly become negligible as the size of $\lambda$ is decreased to values much less than unity. Hence, by appropriately limiting the size of $\lambda$, we may represent the functions adequately with one- or two-term series approximations.

From the general formula (B-2), we write

$$
\begin{aligned}
J_0(\lambda) &= 1 - \frac{\lambda^2}{4} + \frac{\lambda^4}{64} - \cdots , \\
J_1(\lambda) &= \frac{\lambda}{2} - \frac{\lambda^3}{16} + \frac{\lambda^5}{192} - \cdots , \\
J_2(\lambda) &= \frac{\lambda^2}{8} - \frac{\lambda^4}{96} + \cdots , \\
J_3(\lambda) &= \frac{\lambda^3}{48} - \frac{\lambda^5}{768} \cdots , \\
J_4(\lambda) &= \frac{\lambda^4}{384} - \cdots .
\end{aligned}
\tag{B-3}
$$

The procedure we will use is to assume $\lambda$ is small enough that the three-term approximation is very accurate; then we find an upper limit $\lambda_{max}$ of the <u>three</u>-term expression. Accordingly, considering $J_0(\lambda)$, we write

$$
\begin{aligned}
J_{00} &= 1 - \frac{\lambda^2}{4} + \frac{\lambda^4}{64} \quad ; \\
J_{01} &= 1 - \frac{\lambda^2}{4} \quad ; \\
1\% &= 0.01 = \frac{J_{01} - J_{00}}{J_{01}} \\
&= \frac{\frac{\lambda^4}{64}}{1 - \frac{\lambda^2}{4} + \frac{\lambda^4}{64}}
\end{aligned}
\tag{B-4}
$$

Solving this equation for $\lambda$ (taking only the positive real root), we find

$$\lambda = \lambda_{max} = 0.853$$

to insure that $J_{oo}$ is within 1% of $J_{o1}$, and indeed within approximately 1% of the exact value of $J_o(\lambda)$.

Similar calculations are done for $J_1$, $J_2$, and $J_3$; tabulating the results:

$$J_o(\lambda) \cong 1 - \frac{\lambda^2}{4} \qquad \text{for} \quad \lambda \leq 0.853$$

$$J_1(\lambda) \cong \frac{\lambda}{2} \qquad \text{for} \quad \lambda \leq 0.283$$

$$J_2(\lambda) \cong \frac{\lambda^2}{8} \qquad \text{for} \quad \lambda \leq 0.34$$

$$J_3(\lambda) \cong \frac{\lambda^3}{48} \qquad \text{for} \quad \lambda \leq 0.4 \qquad \text{(B-5)}$$

Note that if terms of fourth and higher order in $\lambda$ are neglected, then the Bessel functions of fourth and higher order may all be neglected in the calculations to follow.

We now determine the result of a second modulation of an angle-modulated signal, by treating the signal as an infinite sum of carriers, with each component being modulated separately. For convenience, the following abbreviations will be used:

$e_1$ = once-modulated signal,

$e_2$ = twice-modulated signal, etc.

$J_o = J_o(\lambda)$

$J_1 = J_1(\lambda)$, etc.

$$\omega_{c1} = \omega_c + \omega_m \ ,$$

$$\omega'_{c1} = \omega_c - \omega_m \ ,$$

$$\omega_{c2} = \omega_c + 2\omega_m \ ,$$

$$\omega'_{c2} = \omega_c - 2\omega_m \ , \text{ etc.}$$

Considering the first component of the angle-modulated signal expansion (B-1), and dropping all terms of fourth or higher order in $\lambda$, we find the result of the modulation of this component to be

$$J_o E_c \sin(\omega_c t + \lambda \sin\omega_m t)$$

$$= J_o J_o E_c \sin\omega_c t + J_o J_1 E_c (\sin\omega_{c1} t - \sin\omega'_{c1} t)$$

$$+ J_o J_2 E_c (\sin\omega_{c2} t - \sin\omega'_{c2} t)$$

$$+ J_o J_3 E_c (\sin\omega_{c3} t - \sin\omega'_{c3} t) + \cdots \qquad \text{(B-6)}$$

(Note that succeeding terms would <u>all</u> be of fourth or higher order in $\lambda$, and hence are neglected.)

Considering the first <u>upper sideband</u>, the term $J_1 E_c \sin\omega_{c1} t$ , we find the second modulation gives the result

$$J_1 E_c \sin(\omega_{c1} t + \lambda \sin\omega_m t)$$

$$= J_1 J_o E_c \sin\omega_{c1} t$$

$$+ J_1 J_1 E_c \sin\omega_{c2} t - J_1 J_1 E_c \sin\omega_c t$$

$$+ J_1 J_2 E_c \sin\omega_{c3} t - J_1 J_2 E_c \sin\omega'_{c1} t$$

$$+ \cdots\cdots \qquad \text{(B-7)}$$

The contributions from modulation of the first lower sideband, $- J_1 E_c \sin\omega'_{c1}t$ , are

$$\begin{aligned} & - J_1 E_c \sin(\omega'_{c1}t + \lambda \sin\omega_m t) \\ = & - J_1 J_1 E_c \sin\omega_c t + J_1 J_1 E_c \sin\omega'_{c2}t \\ & - J_1 J_2 E_c \sin\omega_{c1}t + J_1 J_2 E_c \sin\omega'_{c3}t \\ & - \ldots\ldots\ldots \end{aligned} \tag{B-8}$$

From the second upper sideband, we have

$$\begin{aligned} & J_2 E_c \sin(\omega_{c2}t + \lambda \sin\omega_m t) \\ = & J_2 J_o E_c \sin\omega_{c2}t \\ & + J_2 J_1 E_c \sin\omega_{c3}t - J_2 J_1 E_c \sin\omega_{c1}t \\ & + \ldots\ldots\ldots \end{aligned} \tag{B-9}$$

The second lower sideband contributes these terms:

$$\begin{aligned} & - J_2 E_c \sin(\omega'_{c2}t + \lambda \sin\omega_m t) \\ = & - J_2 J_o E_c \sin\omega'_{c2}t \\ & - J_2 J_1 E_c \sin\omega'_{c1}t + J_2 J_1 E_c \sin\omega'_{c3}t \\ & - \ldots\ldots\ldots \end{aligned} \tag{B-10}$$

The third upper sideband contributes only one term of less than fourth order in $\lambda$ :

$$\begin{aligned} & J_3 E_c \sin(\omega_{c3}t + \lambda \sin\omega_m t) \\ = & J_3 J_o E_c \sin\omega_{c3}t + \ldots\ldots \end{aligned} \tag{B-11}$$

The term due to the third lower sideband is:

$$- J_3 E_c \sin(\omega'_{c3} t + \lambda \sin\omega_m t)$$

$$= - J_3 J_o E_c \sin\omega'_{c3} t + \ldots\ldots \qquad \text{(B-12)}$$

All the higher sidebands contribute only terms of higher than third order in $\lambda$.

We collect the coefficients of each frequency component in (B-6) through (B-12) and apply the Bessel-function approximations, dropping again all higher-order terms in $\lambda$, to obtain the following approximate expression for the twice-modulated signal:

$$e_2 \cong (1 - \lambda^2) E_c \sin\omega_c t$$

$$+ (\lambda - \lambda^3/2) E_c \sin\omega_{c1} t - (\lambda - \lambda^3/4) E_c \sin\omega'_{c1} t$$

$$+ \lambda^2/2 E_c \sin\omega_{c2} t - (0) E_c \sin\omega'_{c2} t$$

$$+ \lambda^3/6 E_c \sin\omega_{c3} t - (-\lambda^3/12) E_c \sin\omega'_{c3} t \; . \qquad \text{(B-13)}$$

This expression is now to be compared with the result of modulating a carrier <u>once</u>, with a modulating input of double amplitude (i.e., with $\lambda$ doubled in size.) From the expansion (B-1), using the Bessel-function approximations and replacing $\lambda$ by $2\lambda$, we find this signal to be

$$e_2' \cong (1-\lambda^2)\, E_c \sin\omega_c t$$
$$+ (\lambda - \lambda^3/2)\, E_c\, (\sin\omega_{c1} t - \sin\omega_{c1}' t)$$
$$+ (\lambda^2/2)\, E_c\, (\sin\omega_{c2} t - \sin\omega_{c2}' t)$$
$$+ (\lambda^3/16)\, E_c\, (\sin\omega_{c3} t - \sin\omega_{c3}' t) \qquad \text{(B-14)}$$

We see that if 1) third-order terms in $\lambda$ are also neglected, and 2) all sidebands beyond the <u>first pair</u> may be neglected, then the twice-modulated signal (B-13) is precisely equivalent to $e_2'$ above.

Using the Bessel-function approximations in expansion (B-1) and setting the second-sideband coefficient equal to 1% of the carrier-frequency coefficient, we find that second and higher sidebands may be neglected for

$$\lambda \leq \lambda_{1\ \max} = 0.28\ , \qquad \text{(B-15)}$$

where the subscript 1 indicates that this inequality holds for a <u>single</u> modulation. Obviously, for two-fold modulation, we must have

$$\lambda \leq \lambda_{2\ \max} = \frac{0.28}{2}\ . \qquad \text{(B-16)}$$

For <u>three</u>-fold modulation (that is, another modulation of $e_2$ above), we find that the carrier-frequency component and the first pair of sidebands are identical to the result obtained by a single modulation with a three-times-greater deviation ratio. When a few more steps of calculation are carried out, it becomes clear that for n-fold modulation, retaining consistent approximations, we will have

$$e_n \cong \left(1 - \frac{n^2\lambda^2}{4}\right) E_c \sin\omega_c t$$

$$+ \left(\frac{n\lambda}{2}\right) E_c(\sin\omega_{c1} t - \sin\omega'_{c1} t) \quad , \qquad \text{(B-17)}$$

which is obviously the same as single modulation with a modulating input of amplitude $nE_m$ .

We must still be able to neglect second and higher order sidebands; from (B-15) and (B-16), we see that the condition is

$$\lambda \leq \frac{0.28}{n} \quad , \qquad \text{(B-18)}$$

for n-fold modulation.

(B-18) is the most stringent restriction on $\lambda$ that has been derived; hence it assures the validity of all the other approximations.

In summary, we have shown that n-fold angular modulation is indeed permissible, as long as condition (B-18) above is observed.

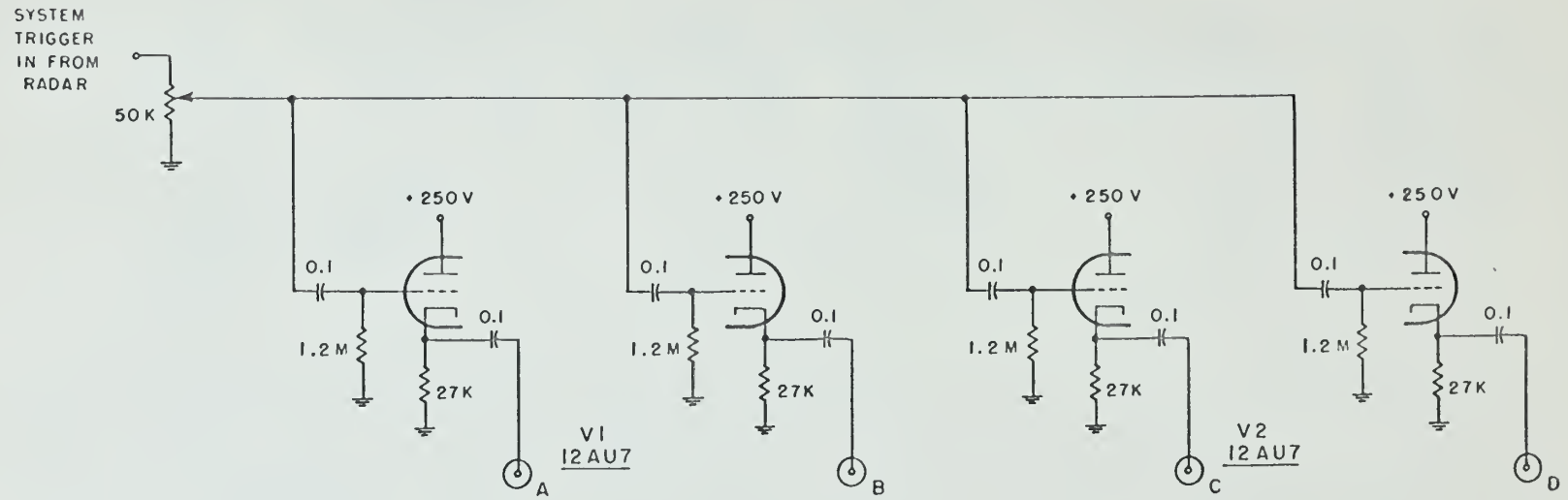


OUTPUTS A, B, C, D ARE FED TO SYSTEM
TRIGGER INPUTS OF THE SWEEP INTEGRATOR

FIG. III-3 SYSTEM TRIGGER CENTRAL

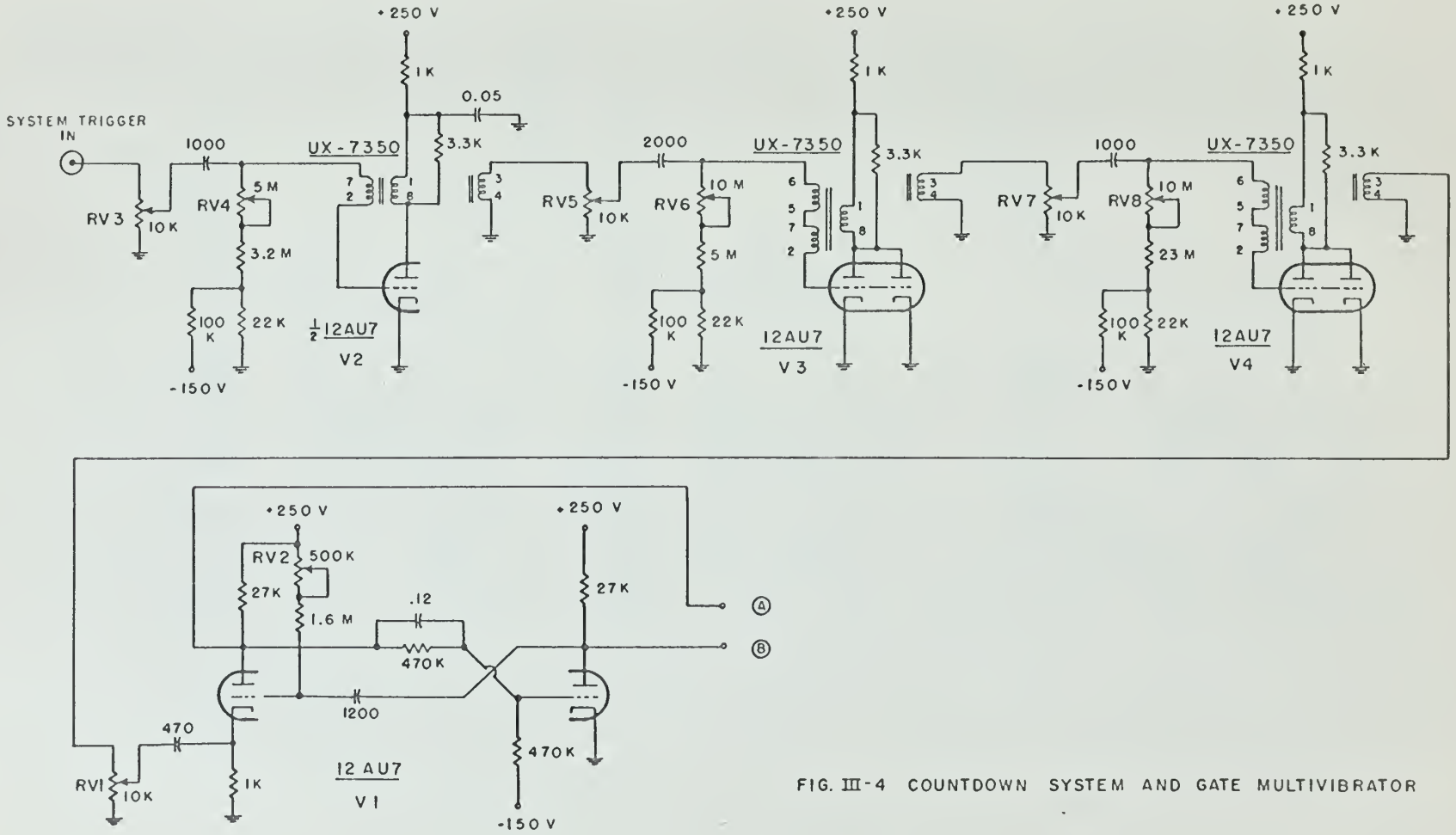


FIG. III-4 COUNTDOWN SYSTEM AND GATE MULTIVIBRATOR

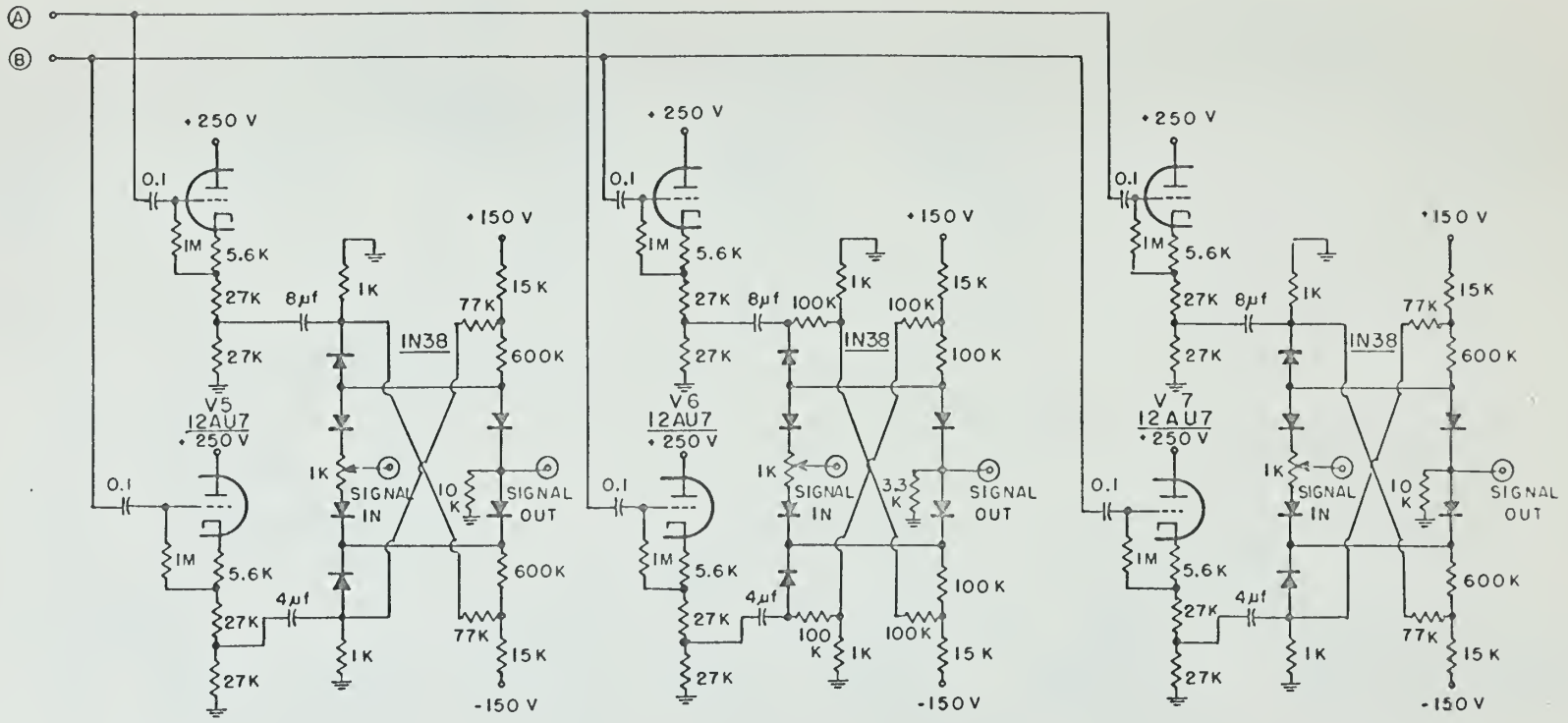


FIG. III-5 GATE SYSTEM

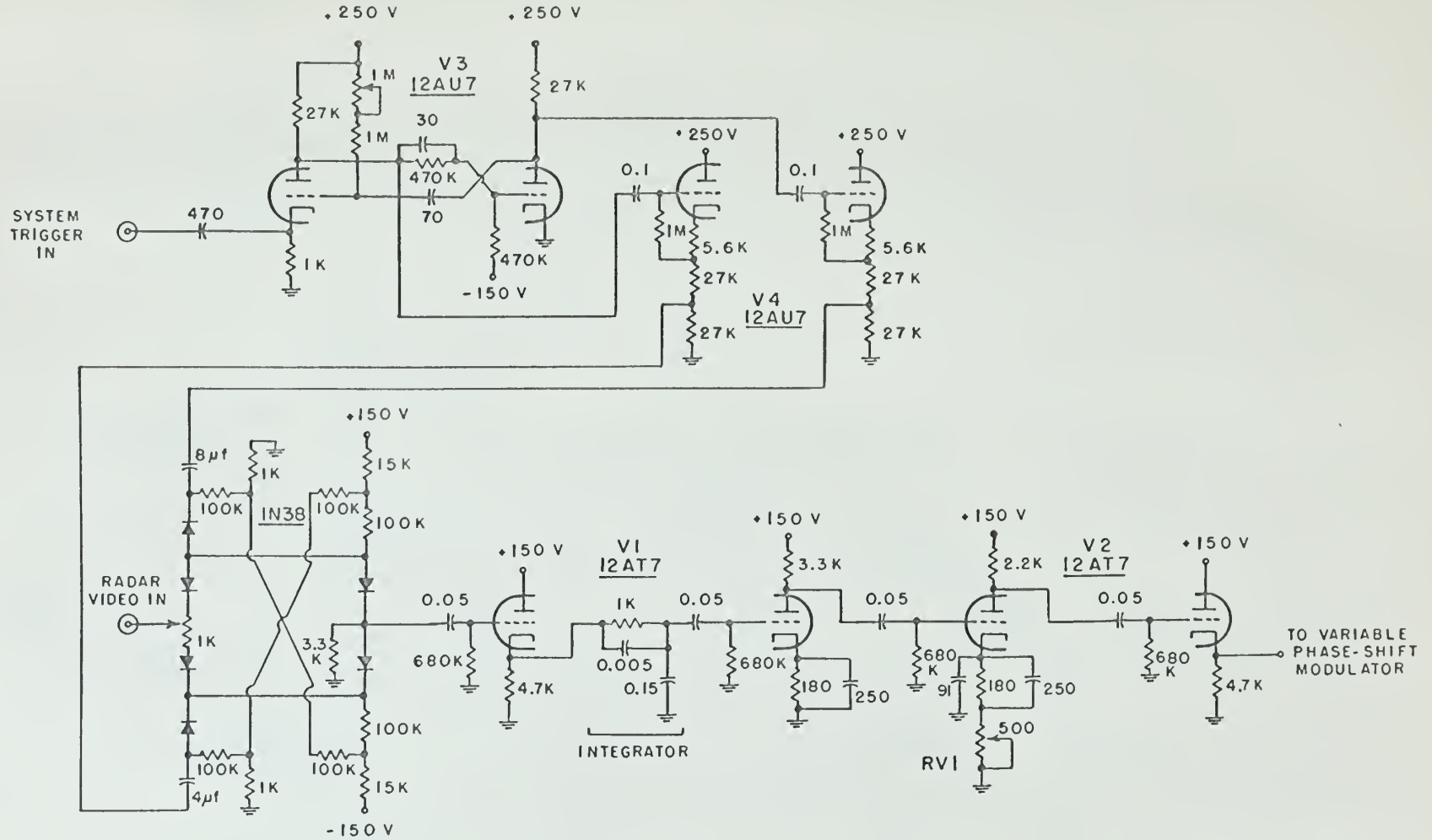


FIG. III-6 6 MILE BLANKING GATE; VIDEO INPUT AMPLIFIER AND INTEGRATOR

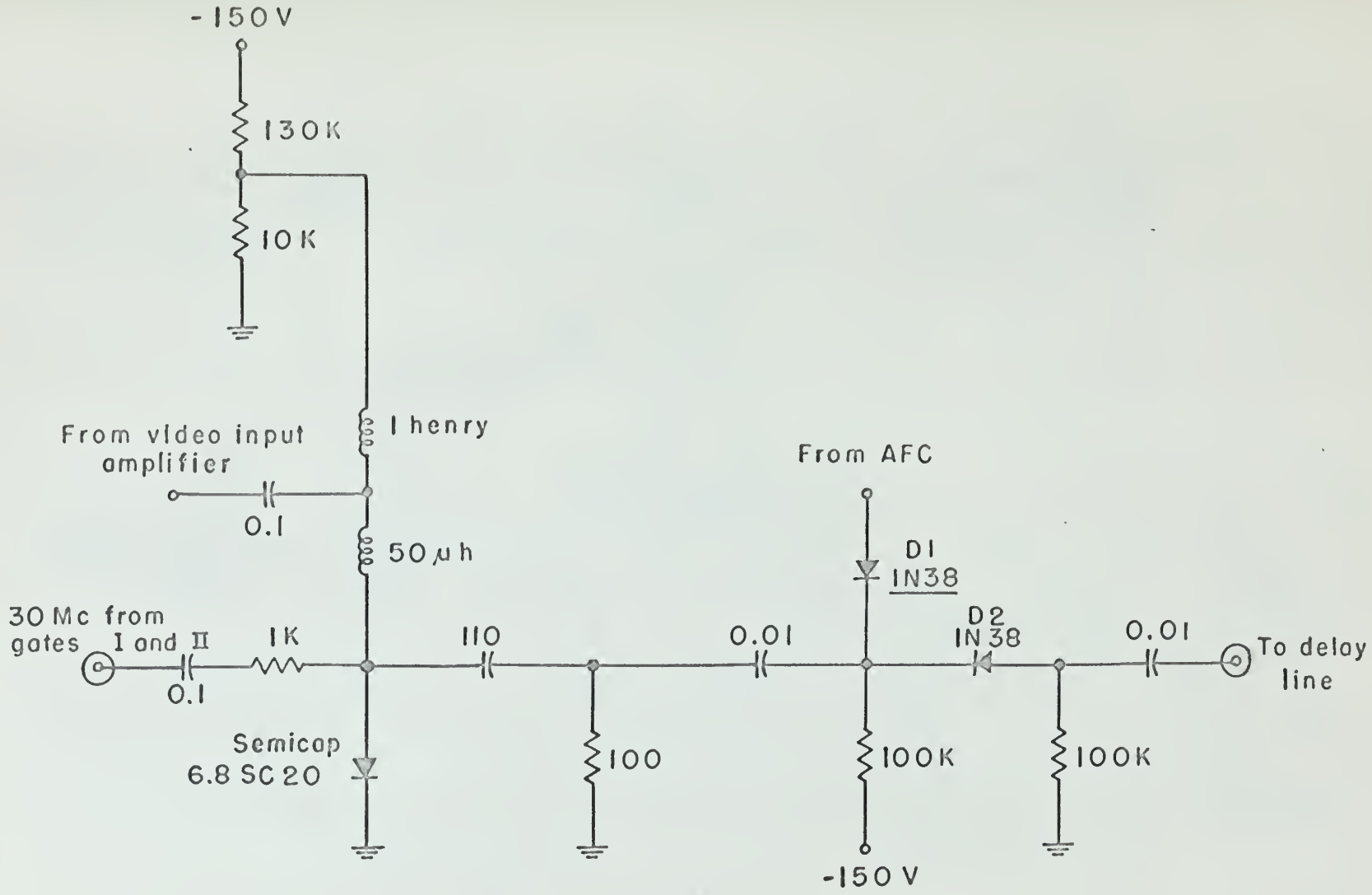


FIG. III-7 VARIABLE-PHASE-SHIFT MODULATOR AND AFC GATE

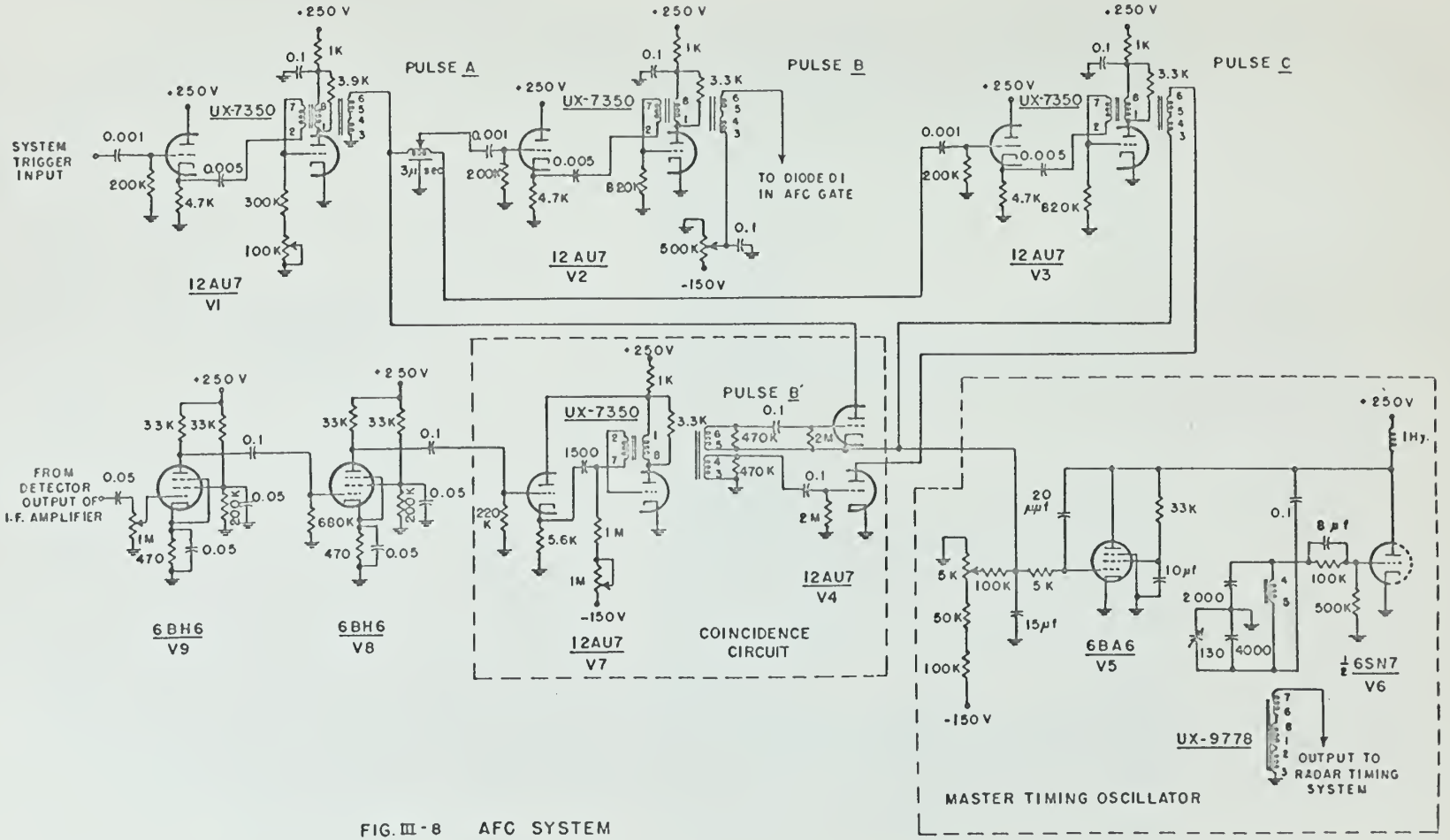


FIG. III-8 AFC SYSTEM

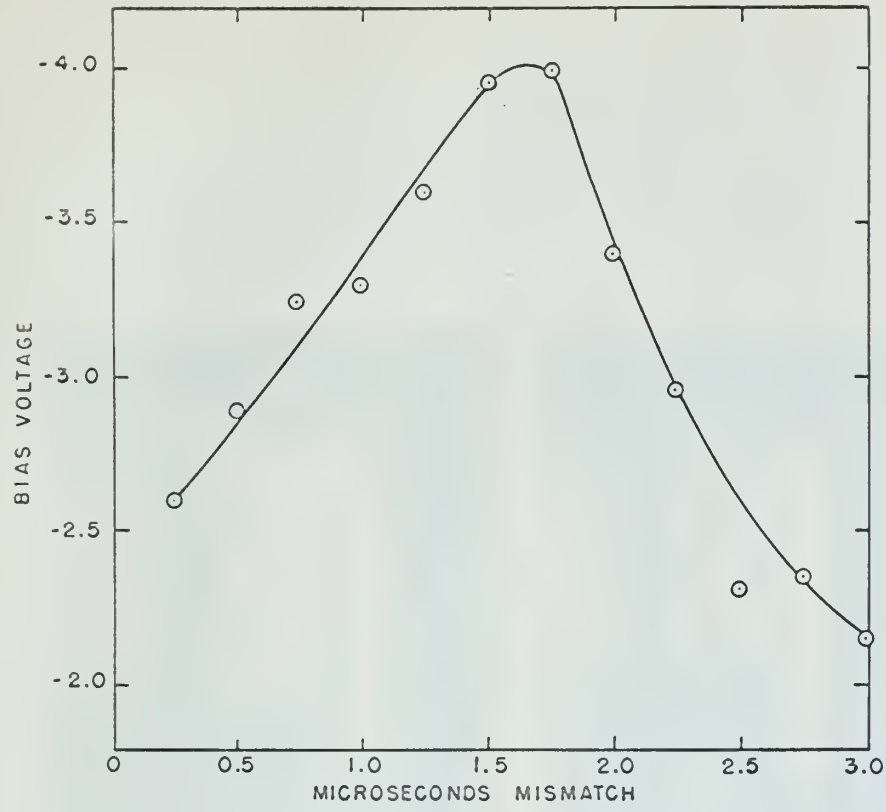


FIG. III-9a AFC CHARACTERISTIC

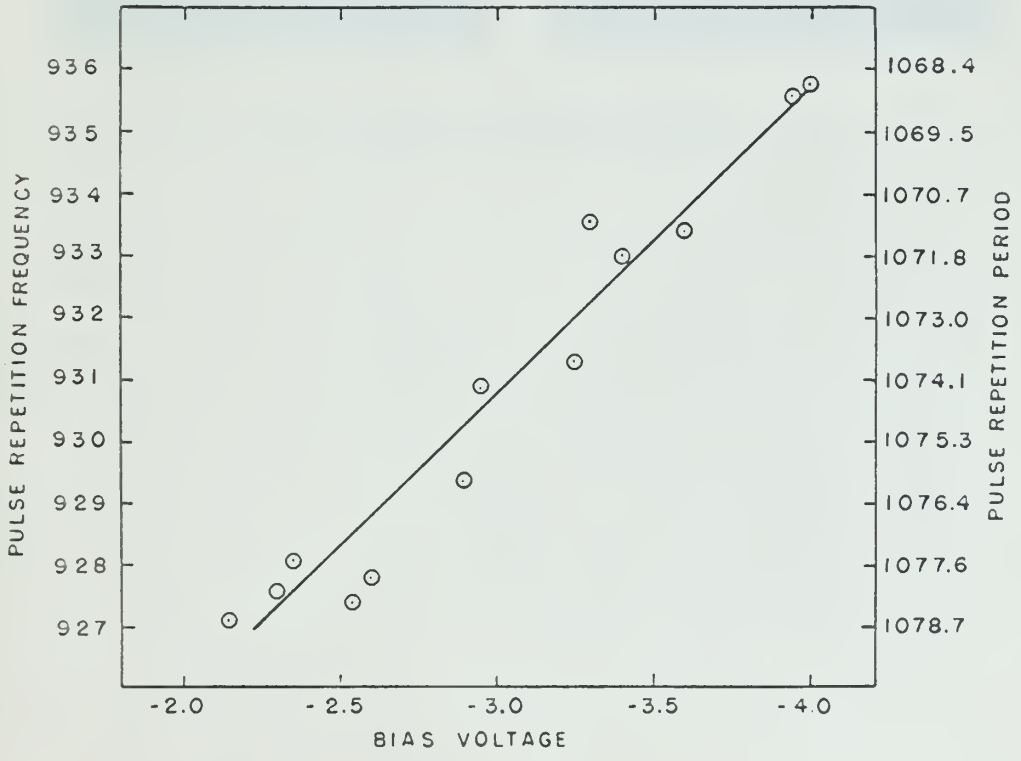


FIG. III-9b MASTER OSCILLATOR CHARACTERISTIC

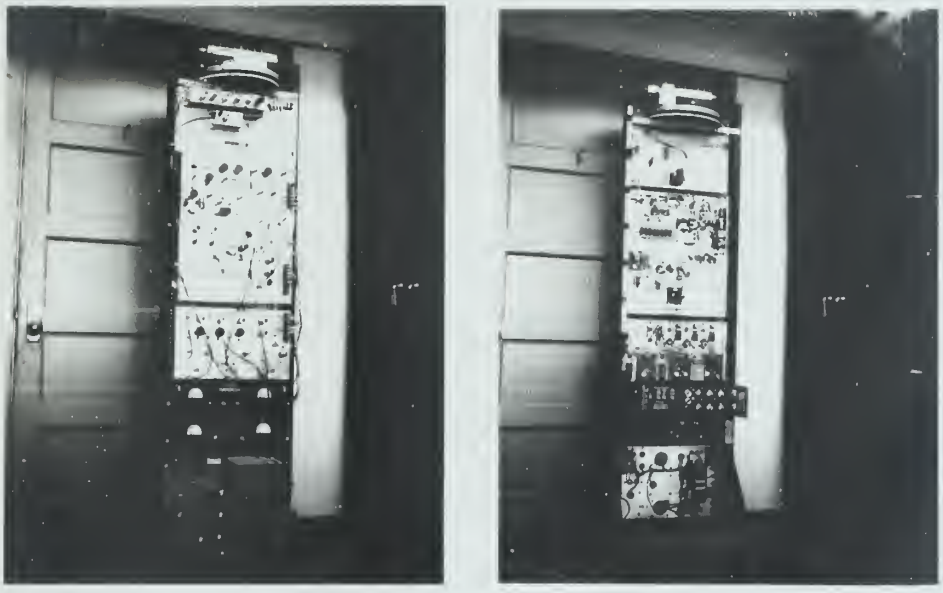

Fig. III-10 The FM Sweep Integrator

## References


(1) Kodaira, N., "Quantitative Mapping of Radar Weather Echoes," Research Report Number 30, June, 1959, Weather Radar Research, Department of Meteorology, M.I.T., pp. 3-5.

(2) Marshall, J. S., and Hitschfeld, W., 1953, "Interpretation of the Fluctuating Echo from Randomly Distributed Scatterers. Part I", Canadian Journal of Physics, Vol. 31: pp. 962-994.

(3) Harrington, J. V., and Rogers, T. F., "Signal-to-Noise Improvement Through Integration in a Storage Tube", Proc. I.R.E., Vol. 38, Number 10, October, 1950.

(4) Philco No. H-1160.1: FM Sweep Integrators, Final Report, Vol. I (Classified)

Philco No. H-1160.2: FM Cancellation Unit, Final Report, Vol. II (Classified)

Philco No. H-1160.4: Video Data Processor, Final Report (Classified)

Philco No. H-1160.4HB: Supplement to Instruction Guide for Video Data Processor (Classified)

Philco Proposal R-209: FM Transmission for Continuous Cancellation and Sweep Integration Filters (Classified)

(5) General Atronics Corporation, "The Atronics Model SR Video Sweep Integrator," May, 1959.

(6) Kodaira, N., op. cit., pp. 5-13

(7) Kodaira, N., op. cit., pp. 8-9

(8) Hund, A., "Frequency Modulation", McGraw-Hill, New York, 1942.

(9) Goldsmith, A. N., et. al., "Frequency Modulation, Volume I", RCA Review, Princeton, N.J., January, 1948.

(10) Marchand, N., "Frequency Modulation", Murray Hill, New York, 1948.

(11) Giacoletto, L. J., "Generalized Theory of Multitone Amplitude and Frequency Modulation", Proceedings of the I.R.E., Volume 35, Number 7, July, 1947.

(12) Hund, A., op. cit., pp. 121-122

(13) Millman and Taub, "Pulse and Digital Circuits", McGraw-Hill, New York, 1956, pp. 445-447.

(14) Kodaira, N., op. cit., p. 33.